Experimental investigation of shear-induced migration in particle-laden pipe flow using MRI

Hogendoorn, Willian; Frank, David; Bruschewski, Martin; Poelma, Christian

Publication date
2022

Document Version
Final published version

Citation (APA)
Hogendoorn, W., Frank, D., Bruschewski, M., & Poelma, C. (2022). *Experimental investigation of shear-induced migration in particle-laden pipe flow using MRI*. Paper presented at 12th International Symposium on Turbulence and Shear Flow Phenomena, TSFP 2022, Osaka, Virtual, Japan.

12th International Symposium on Turbulence and Shear Flow Phenomena (TSFP12)
Osaka, Japan, July 19–22, 2022

EXPERIMENTAL INVESTIGATION OF SHEAR-INDUCED MIGRATION IN PARTICLE-LADEN PIPE FLOW USING MRI

Willian Hogendoorn
Multiphase Systems (3ME-P&E)
Delft University of Technology
Leeghwaterstraat 39, 2628 CB Delft, The Netherlands
w.j.hogendoorn@tudelft.nl

David Frank
Lehrstuhl Strömingsmechanik
Universität Rostock
Albert-Einstein-Str. 2, 18059 Rostock, Germany
david.frank@uni-rostock.de

Martin Bruschewski
Lehrstuhl Strömingsmechanik
Universität Rostock
Albert-Einstein-Str. 2, 18059 Rostock, Germany
martin.bruschewski@uni-rostock.de

Christian Poelma
Multiphase Systems (3ME-P&E)
Delft University of Technology
Leeghwaterstraat 39, 2628 CB Delft, The Netherlands
c.poelma@tudelft.nl

ABSTRACT

Using magnetic resonance imaging we are able to obtain average velocity and volume fraction profiles in a pipe flow with a neutrally buoyant suspension. In this experimental work, the effect of increasing Reynolds number and particle volume fraction on shear-induced migration is studied. For increasing bulk volume fraction, the initially nearly homogeneous suspension gradually changes to a strongly non-homogeneous suspension. This is observed for all studied Reynolds numbers. In contrast to the majority of previous (MRI) studies, experiments are also performed for suspension Reynolds numbers of approximately 5000 in order to study inertial effects on shear-induced migration.

INTRODUCTION

Particle-laden flows are gaining a growing and continuous interest over the last decades (Guazzelli & Pouliquen, 2018; Morris, 2020). This interest is motivated by the relevance of these suspensions in industrial, geophysical and societal contexts. A variety of practical applications include the food processing industry, 3D bioprinting of organs, and sediment transport. The modeling of suspension flow dynamics in moderate and concentrated regimes is considered to be a challenge, in particular when inertial effects cannot longer be ignored. Despite significant theoretical, experimental and numerical progress, open questions still remain. In this experimental work a systematic study is conducted to investigate the effect of the Reynolds number (Re) and particle volume fraction (ϕ) on shear-induced migration. To this end, magnetic resonance imaging (MRI) experiments are performed on a neutrally-buoyant particle-laden system. In contrast to other experimental techniques, MRI allows for accurate measurements in dense suspensions, where velocity and volume fractions can be simultaneously measured.

Shear-induced migration will be observed when studying suspension flow dynamics in shear flows. Finite-sized particles experience a force resulting from the velocity gradient: an initially homogeneous suspension rearranges to a non-homogeneous mixture. Particle clusters are formed along the direction of the velocity gradient, where the particles are transported in the direction of decreasing shear rate. These concentration gradients are subsequently responsible for (strong) viscosity gradients. Therefore, the effective viscosity needs to be modelled as a local viscosity instead of a constant viscosity for particle-laden shear flows (Gadala-Maria & Acrivos, 1980). The phenomena of shear-induced migration is observed in a variety of flow configurations, including Couette systems (Gadala-Maria & Acrivos, 1980; Abbott *et al.*, 1991; Blanc *et al.*, 2013), channel flows (Lyon & Leal, 1998; Zade *et al.*, 2018) and pipe flows (Altobelli *et al.*, 1991; Sinton & Chow, 1991). In addition to experimental work, theoretical models were introduced by Leighton & Acrivos (1987) and Phillips *et al.* (1992) in order to explain the experimental observations. Furthermore, a suspension balance model (SBM) was introduced by Nott & Brady (1994). In a revision of this model, a well-defined particle phase stress is added, instead of the identification of the particle phase stress with the particle contribution to the suspension stress (Nott *et al.*, 2011). By taking this particle stress contribution into account, this model is distinct from other models, which only take into account a force acting on the particle phase. However, experimental and theoretical studies are predominantly limited to the Stokesian regime in order to avoid inertial effects, as these effects will further complicate the modeling efforts. In this study experiments are performed for a range of Reynolds numbers, spanning the laminar, transitional and turbulent region, as for many practical applications inertial effects cannot be neglected. Furthermore, in order to resolve discrepancies between numerical and experimental studies, a reliable experimental data set will significantly aid the the validation and development of numerical models.

EXPERIMENTAL DETAILS

Experiments are performed in a 30.35 ± 0.12 mm diameter (D) pipe flow setup using unexpanded polystyrene particles (Synthos EPS) with a diameter, $d = 1.75 \pm 0.12$ mm, resulting in a particle-to-pipe diameter ratio, $d/D = 0.058$. For the continuous phase a glycerol-water mixture (13.6/86.4%) is used

Table 1: Used MRI parameters

Parameter	**Value**
Matrix size	$640 \times 640 \times 1$
Non-isotropic resolution	$0.3 \times 0.3 \times 50$ mm^3
Repetition time (TR)	22 ms
Echo time (TE)	9 ms
RF flip angle	5°
Receiver bandwidth	280 Hz/pixel
Velocity Encoding	0.1 –1.7 m/s
Number of averages	32

in order to match the density of the fluid with the particles, ρ = 1032±1.17 kg/m^3. Furthermore, coppersulfate ($CuSO_4$; 1g/L) is added in order to enhance the signal-to-noise ratio of the MRI measurements. A progressive cavity pump (AxFlow B.V., Lelystad, the Netherlands) is used to transport the suspension. The flowloop is constructed as follows: first, a settling chamber is used. An orifice is placed 10D after this settling chamber in order to ensure a transition at a fixed critical Reynolds number, $Re_c \approx 2000$ for single-phase flows. Note that this onset of turbulence for particle-laden flows is a function of d/D and the volume fraction, ϕ (Hogendoorn *et al.*, 2022). MRI measurements are obtained at a downstream distance of 132D from this orifice. The flowrate is monitored using an inline Coriolis mass flow meter (KROHNE OPTIMASS 7050c), which is located in the return section. This return loop is connected to a reservoir, closing the flow loop, as the pump is fed from this reservoir. In order to be able to achieve low Reynolds numbers in the system, a bypass is installed from the pump exit to the reservoir. Additionally, a valve is placed in the main flow loop to be able to reduce the Reynolds number even further. A cooling system (JULABO FT 402) is used to minimise the temperature increase of the suspension from heat addition by the pump. Particles are added in steps of 10% until a volume fraction of 50%. In addition, experiments are performed for a volume fraction of 45%. Experiments are performed for three different target Reynolds numbers of 800, 2000 and 5000.

A MAGNETOM Trio 3T Whole-Body MRI scanner (Siemens, Erlangen, Germany) is used to obtain velocity and concentration data. This system has a maximum gradient amplitude of 40 mT/m and a maximum gradient slew rate of 200 T/m/s. Two standard receive-only body coils were used to receive the signal, with a receiver bandwidth of 280 Hz/pixel. Repetition (TR) and echo (TE) times of respectively 22 and 9 ms are used, in combination with a RF flip angle of 5°. A non-isotropic resolution of $0.3\times0.3\times50$ mm^3 is used in the x, y, and z direction, respectively. The z component is in the streamwise direction. The $x-y$ plane is perpendicular to the streamwise direction with x the horizontal and y the vertical component. The used parameters are summarised in Table 1.

In order to validate the complete experimental setup and the MRI system, experiments are compared with reference data from literature. To this end single-phase experiments are performed for Re = 5300, 10000, and 25000, for which average velocity profiles are available. A total average error (averaged along the radial direction) between the mean velocity profiles of less than 1% is found. Furthermore, the error in the volume fraction is determined using error propagation (Bruschewski *et al.*, 2016). For all 19 cases studied a maximum error of 2.3% is found. The order of magnitude of this error is confirmed by comparing the integrated volume fraction profiles with the target bulk volume fraction set by preparing the suspension. For the highest volume fraction case (ϕ = 0.5), a discrepancy of 2.7% is found, as the integrated volume fraction was determined to be 0.473. Note that this error comprises all experimental and measurement uncertainties, i.e., errors when preparing the suspension, inhomogeneities in the system, calibration errors of the MRI system, reconstruction errors, etc. The actual bulk volume fraction in the pipe is particularly important for the determination of the corresponding suspension based Reynolds number (Re_s). This Reynolds number is based on the effective suspension dynamic viscosity, μ_s, which is determined using Eilers's viscosity correction (Eilers, 1941):

$$\frac{\mu_s}{\mu_0} = \left(1 + 1.25\frac{\phi}{1-\phi/\phi_m}\right)^2. \tag{1}$$

Here μ_0 is the viscosity of the single-phase fluid, in our case a glycerol-water mixture. For the maximum packing fraction, ϕ_m, a value of 0.64 is used. In previous studies this value is shown to be an appropriate choice for our batch of particles (Hogendoorn & Poelma, 2018; Hogendoorn *et al.*, 2021). Furthermore, the volume fraction used to determine the apparent viscosity is based on the integrated volume fraction profile, as this is considered to result in a more accurate determination of Re_s. This in contrast of using the mass fraction of the particles and fluid when preparing the suspension, as due to the radial concentration gradients the apparent volume fraction in the pipe differs from the bulk volume fraction in the main reservoir. Also, the average volume fractions reported in this study are based on the same integrated volume fraction profiles.

RESULTS

A schematic overview of all conducted experiments, including the single-phase validation experiments, are shown in Fig. 1. The marker color indicate the corresponding particle perturbation amplitude, $\varepsilon = \left(\frac{d}{D}\right)^{\frac{1}{2}}\phi^{\frac{1}{6}}$, as introduced by Hogendoorn *et al.* (2022). This parameter was shown to distinguish between different transition scenarios and allows a prediction of the onset of turbulence for a range of suspensions. The three different target Reynolds numbers (i.e., Re_s = 800, 2000, and 5000) are indicated by the horizontal dashed lines. The deviation of the actual measurements from the target Reynolds numbers is due to the fact that the actual volume fraction in the measurement section is determined *a posteriori*. This is done by circumferential integration of the particle volume fraction profile, obtained from the MRI measurements. This method is considered to result in a more accurate determination of the bulk volume fraction, rather than using the mass fractions of the fluid and solid phase when preparing the suspension (see also the discussion in the validation section). Note that the suspension Reynolds number is also affected by the determined bulk volume fraction.

The average velocity and concentration profiles for an approximate suspension Reynolds number of 2000 are shown in Fig. 2a and Fig. 2b, respectively. For this selected Reynolds number several observations can be made. First, for increasing volume fraction, the velocity profiles gradually changes

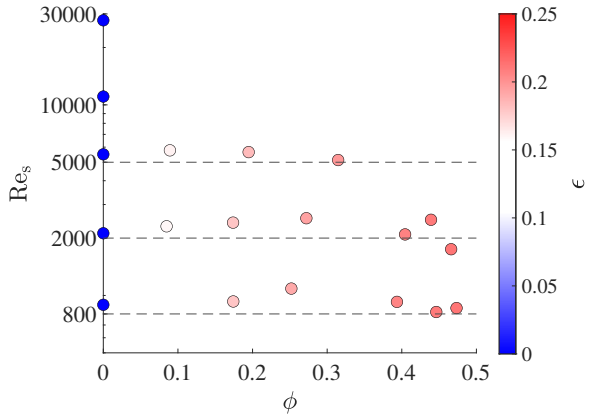

Figure 1: Schematic overview of performed experiments, as function of Re_s and ϕ. The marker color indicate the particle perturbation amplitude, ε.

from a parabolic profile to a blunted profile, eventually resulting in a uniform velocity in the pipe center for the case with $\phi_b = 0.47$. Note that the velocity profile corresponding to $Re_s = 2307$, $\phi_b = 0.08$ deviates from this trend. This is most likely explained by the change in transition mechanism which occurs for these specific conditions (Hogendoorn & Poelma, 2018; Hogendoorn *et al.*, 2021). Also, from the corresponding volume fractions profiles in Fig. 2b, it can be seen that the particle distribution for this specific case is nearly uniform. For increasing volume fraction this nearly homogeneous suspension gradually changes to a strongly non-homogeneous suspension (see, e.g., $\phi_b \geq 0.27$). This suggest that particle-particle interactions are playing an important role in the suspension dynamics (see, e.g., Guazzelli & Pouliquen, 2018). Additionally, the local shear-rate will be an important parameter for the volume fraction distribution. The volume fraction profiles also explains the (degree of) blunting of the velocity profiles for increasing ϕ_b. For $\phi_b > 0.27$ the particle distribution in the pipe center is found to be approaching the random close packing, which is inherently ordered and restricts shear. In the direction of the pipe wall, the volume fraction decreases. This results in a (more) dis-ordered system, allowing more shear; this is also visible in the velocity profiles. Eventually, in the near-wall region ($r/D \approx 0.47$) a concentration 'peak' can be observed for the dense cases. This ordered particle layer was observed before by e.g., Hampton *et al.* (1997). The peak becomes more pronounced for increasing ϕ_b. Moreover, additional particle rings can be observed, as can be interpreted from the additional 'wiggles' in the profiles of the dense cases.

These particle rings are even better visible for the highest volume fraction experiment at a lower Re_s. The average velocity and volume fraction profile are shown in Fig. 3a. The velocity profile is normalised using the bulk velocity and corresponds to the left y-axis, whereas the average volume fraction profile corresponds to the right y-axis. A pipe cross-section of the particle distribution is shown in the 2D grayscale map of the volume fraction in Fig. 3b. This contains similar information as the average volume fraction profile.

CONCLUSION AND OUTLOOK

The effect of increasing volume fraction and Reynolds numbers is studied on shear-induced migration. Average velocity and concentration profiles are obtained for neutrally buoyant particle-laden pipe flow using MRI. Shear-induced migration is observed for a range of Reynolds numbers. For increasing volume fraction, the initially nearly homogeneous suspension gradually changes to a strongly non-homogeneous suspension. This shows that particle-particle interactions play an important role in the underlying dynamics. In particular for $\phi_b \geq 0.27$ a dense particle core is observed, explaining the observed blunted velocity profiles. Currently, direct numerical simulations are pursued in order to explain the obtained velocity and volume fraction profiles and to distinguish between the different contributions involved.

REFERENCES

Abbott, JR, Tetlow, N, Graham, AL, Altobelli, SA, Fukushima, Eiichi, Mondy, LA & Stephens, TS 1991 Experimental observations of particle migration in concentrated suspensions: Couette flow. *Journal of rheology* **35** (5), 773–795.

Altobelli, SA, Givler, RC & Fukushima, Eiichi 1991 Velocity and concentration measurements of suspensions by nuclear magnetic resonance imaging. *Journal of Rheology* **35** (5), 721–734.

Blanc, Frédéric, Lemaire, Elisabeth, Meunier, Alain & Peters, François 2013 Microstructure in sheared non-Brownian concentrated suspensions. *Journal of rheology* **57** (1), 273–292.

Bruschewski, Martin, Freudenhammer, Daniel, Buchenberg, Waltraud B, Schiffer, Heinz-Peter & Grundmann, Sven 2016 Estimation of the measurement uncertainty in magnetic resonance velocimetry based on statistical models. *Experiments in Fluids* **57** (5), 1–13.

Eilers, von H 1941 Die viskosität von emulsionen hochviskoser stoffe als funktion der konzentration. *Kolloid-Zeitschrift* **97** (3), 313–321.

Gadala-Maria, F & Acrivos, Andreas 1980 Shear-induced structure in a concentrated suspension of solid spheres. *Journal of Rheology* **24** (6), 799–814.

Guazzelli, Elisabeth & Pouliquen, Olivier 2018 Rheology of dense granular suspensions. *Journal of Fluid Mechanics* **852**.

Hampton, RE, Mammoli, AA, Graham, AL, Tetlow, N & Altobelli, SA 1997 Migration of particles undergoing pressure-driven flow in a circular conduit. *Journal of Rheology* **41** (3), 621–640.

Hogendoorn, Willian, Chandra, Bidhan & Poelma, Christian 2021 Suspension dynamics in transitional pipe flow. *Physical Review Fluids* **6** (6), 064301.

Hogendoorn, Willian, Chandra, Bidhan & Poelma, Christian 2022 Onset of turbulence in particle-laden pipe flows. *Phys. Rev. Fluids* **7**, L042301.

Hogendoorn, Willian & Poelma, Christian 2018 Particle-laden pipe flows at high volume fractions show transition without puffs. *Physical Review Letters* **121** (19), 194501.

Leighton, David & Acrivos, Andreas 1987 The shear-induced migration of particles in concentrated suspensions. *Journal of Fluid Mechanics* **181**, 415–439.

Lyon, MK & Leal, LG 1998 An experimental study of the motion of concentrated suspensions in two-dimensional channel flow. Part 1. Monodisperse systems. *Journal of fluid mechanics* **363**, 25–56.

Morris, Jeffrey F. 2020 Toward a fluid mechanics of suspensions. *Phys. Rev. Fluids* **5**, 110519.

Nott, Prabhu R & Brady, John F 1994 Pressure-driven flow of suspensions: simulation and theory. *Journal of Fluid Mechanics* **275**, 157–199.

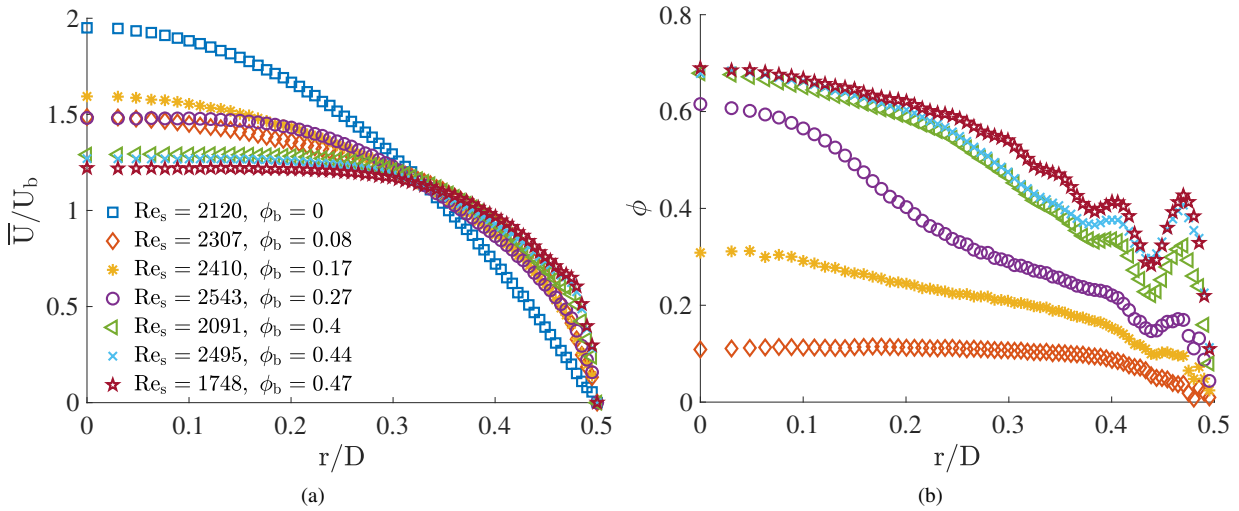

Figure 2: (a) Normalised average velocity profiles as function of the pipe radius for approximately constant suspension Reynolds number, $Re_s \approx 2000$, and increasing volume fraction. (b) Average concentration profiles as function of the pipe radius. The markers are corresponding to the conditions indicated in the legend in Fig. 2a.

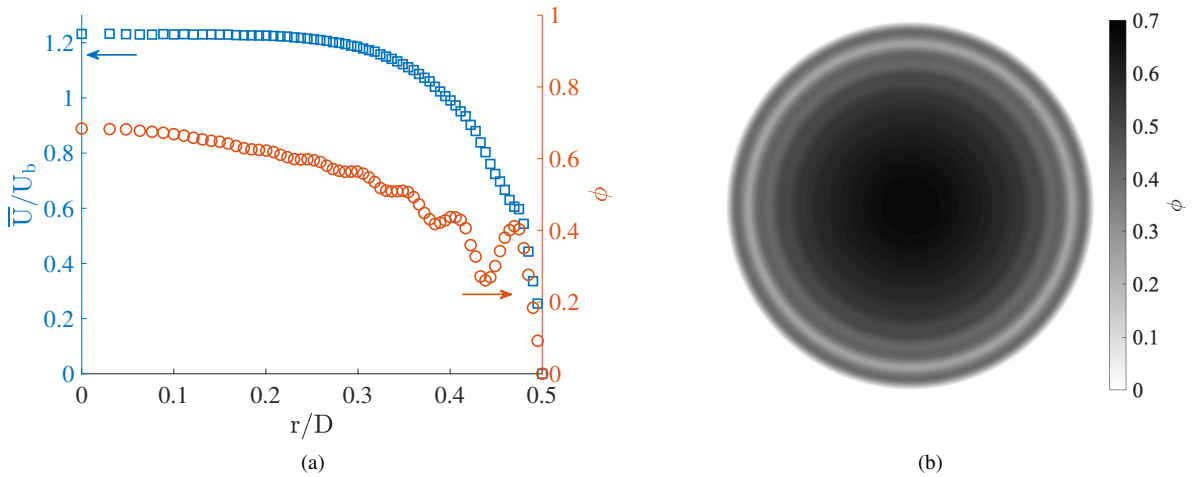

Figure 3: (a) Normalised average velocity profile (blue squares, left y-axis) and average volume fraction profile (red circles, right y-axis) as function of the pipe radius for a suspension Reynolds number, Re_s = 859, and bulk volume fraction, ϕ_b = 0.473. (b) 2D map of the volume fraction corresponding to the profile of Fig. 3a.

Nott, Prabhu R, Guazzelli, Elisabeth & Pouliquen, Olivier 2011 The suspension balance model revisited. *Physics of Fluids* **23** (4), 043304.

Phillips, Ronald J, Armstrong, Robert C, Brown, Robert A, Graham, Alan L & Abbott, James R 1992 A constitutive equation for concentrated suspensions that accounts for shear-induced particle migration. *Physics of Fluids A: Fluid Dynamics* **4** (1), 30–40.

Sinton, Steven W & Chow, Andrea W 1991 NMR flow imaging of fluids and solid suspensions in Poiseuille flow. *Journal of Rheology* **35** (5), 735–772.

Zade, Sagar, Costa, Pedro, Fornari, Walter, Lundell, Fredrik & Brandt, Luca 2018 Experimental investigation of turbulent suspensions of spherical particles in a square duct. *Journal of Fluid Mechanics* **857**, 748–783.